SECOND EUROPEAN CONFERENCE ON EARTHQUAKE ENGINEERING
AND SEISMOLOGY, ISTANBUL AUG. 25-29, 2014

A STUDY ON HIGH FREQUENCY EXCITATIONS OF SLIDING BASE ISOLATED BUILDING UNDER SEISMIC EXCITATION

SANJUKTA CHAKRABORTY and SAMIT RAY-CHAUDHURI

ABSTRACT

Previous studies have demonstrated that a sudden change in stiffness of a building (due to sudden sliding or nonlinear deformation of members) may result in an increase in the floor level responses than that for the same building modelled as a linear structure. It has also been demonstrated that this phenomenon occurs as a result of excitation of high frequency modes as a result of energy transfer from the lower (and excited) modes. In this work, a systematic study is carried to understand and evaluate the energy transfer by formulating the equations of motions for different phases of motions. For simplicity, an initial velocity profile, proportional to the fundamental mode of a multi-degree-of-freedom (MDOF) system, is considered and the free-vibration response of the system is studied. A numerical investigation is then carried out wherein the influence of different parameters on the energy transfer to different modes of a system undergoing hysteresis is studied. Further, simplified approximate expressions by adopting a perturbation approach are also obtained to understand the contribution of different terms. Finally, the accuracy of the simplified expressions is evaluated so that these expressions can be used for evaluation of modal energy at different stages of hysteresis.

INTRODUCTION

It has now been well established that base isolation is one of the most effective strategy to control the seismic response of a building. Of particular interest is the sliding base isolation system. When subjected to ground excitation, a structure isolated by sliding bearings exhibits a stiff behaviour initially and as the excitation exceeds certain limit, the structure starts sliding. This stick-slip behaviour can be idealized as an elasto-plastic hysteretic type where a huge amount of seismic energy is dissipated due to the hysteresis. The energy dissipation through hysteresis is an intended mechanism as well for a fixed base structure that is designed to go in to its nonlinear zone during moderate to strong earthquakes.

Previous studies have demonstrated that the deformation of buildings beyond their linear zone (resulting in a sudden change in stiffness) may result in an increase in the floor response spectrum ordinates (of any floor) than that for the same building modelled as a linear structure. Swell et al. (1989) and Singh et al. (1996) stated that this phenomenon occurs because of the excitation of high frequency modes due to the nonlinearity in structures. Rodriguez et al. (2002) also found that there may be a higher amplification of absolute acceleration at lower floor levels of a nonlinear RC building than that of the same building modelled as a linear structure. In a recent study involving a building isolated with flat sliding bearings, Chakraborty et al. (2012) demonstrated that there is an increase in the contribution of high frequency modes in floor level responses once the building starts sliding (i.e., due to a sudden change in the stiffness of the system). In addition, the base displacement and base shear time-histories, and the PFA (peak-floor-acceleration) distribution along the height of the isolated building displayed the presence of high frequency contribution after the building starts sliding.

The increase in floor response due to excitation of high frequency modes as observed from the aforementioned studies may be a cause for non-structural damage in previous earthquakes (2008). Many studies have been carried out on the interaction of the nonstructural components and their supporting structures. The interaction effect on a non-structural component is significant when some of the structural frequencies match with that of the non-structural component. For a building hosting various essential equipment, such a tuning condition is avoided by keeping the fundamental frequency of the building away from the equipment frequencies. The excitation of the high frequency modes may however cause a frequency tuning.

Several studies on the hysteretic systems had been carried in the past and these are not listed here to save space. However, the primary focus of those studies was on the estimation of steady state response under harmonic loading. As per authors' knowledge, no systematic investigation has been carried out so far on the energy transfer phenomenon of a hysteretic system. In this work, the energy transfer among modes of an MDOF system possessing hysteretic behaviour is studied.

FORMULATION

A base isolated structure with or without any restoring mechanism, undergoes stiffness degradation when subjected to sudden slip during a strong earthquake excitation. A building isolated using sliding isolators can be modelled as a bilinear hysteretic system. Figure 1 provides a schematic diagram of an n-story isolated building. In Figure 1, x_i, m_i and k_i respectively represent the relative displacement of the i^{th} story with respect to the ground, mass of the i^{th} story and the i^{th} story stiffness. The displacement of the isolator with respect to the ground is represented by x_b. The coefficient of friction between the ground and slider is considered as μ. The slider demonstrates two phases: sticking phase and sliding phase. The condition for sticking phase is $k_1(x_1 - x_b) < \mu W$, where W is the total weight of the building. The relative displacement of the slider x_b is zero at the beginning of ground motion. Considering an un-damped system, the equation of motion during the sticking phase can be described as follows:

$$[M]\{\ddot{x}\} + [K]\{x\} = -[M]\{\ddot{x}_g\} \tag{1}$$

where $[M]$, and $[K]$ are the mass and stiffness matrix of the system, respectively. Once $k_1(x_1 - x_b)$ exceeds μW with W being the seismic weight of the system, sliding phase starts. This sliding phase continues until $\dot{x}_1$ becomes zero. Figure 2 provides a schematic diagram of the stick-slip behaviour showing a plot of displacement at the first floor versus force in a bottom column. It is obvious from this plot that the behaviour of the sliding isolation system is exactly similar to an elasto-plastic hysteretic system.
In this study, a spring-mass idealization of a sliding base isolated building is considered. The spring nearest to the support is considered to be bilinear with hysteretic behaviour to make the system similar to a sliding isolator. The idealized system is shown in Figure 3, where the symbols used are same as that in Figure 1 except with the addition of β as strain hardening ratio for the spring connected to the support.

In this work, the modal energy dissipation and transfer related phenomena are studied under an initial velocity condition such that the initial velocity profile is proportional to a particular mode (say, j^{th} mode) of the MDOF system. For this purpose, a hysteretic half-cycle is divided in three stages as described in Figure 4. The first stage corresponds to the initial stiffness of the bilinear spring. In this stage, all the energy will be in the j^{th} mode as it was excited with an initial velocity. At the second stage, the system enters into the stiffness degraded zone. In this zone, as a result of stiffness degradation, the modal properties of the system change. Consequently, as a result of modal coupling (see Ray-Chaudhuri, 2007), all the modes (represented by degraded stiffness) get excited. In the third stage, the system again comes back to the initial stiffness zone with the initial modal properties.

During this transition from Stage 2 to Stage 3, some energy gets dissipated along with alteration of energy content of corresponding modes.

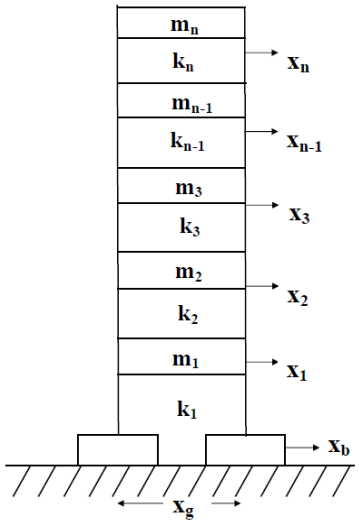

Figure 1: Building with sliding isolator

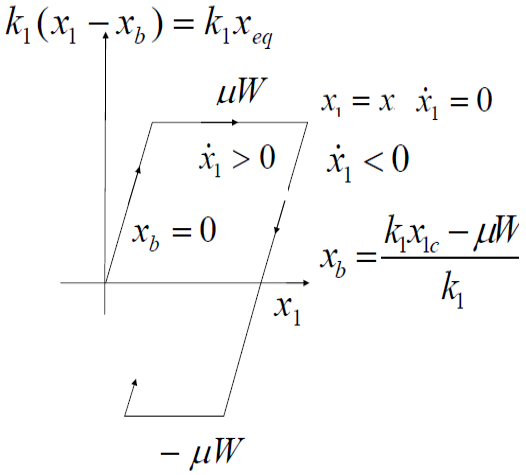

Figure 2: Stick-slip behaviour of sliding isolator

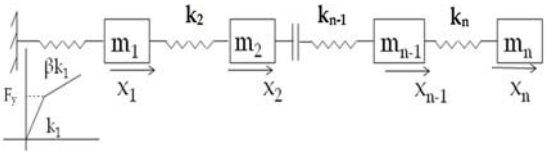

Figure 3: Spring-mass idealization of a sliding base isolated building

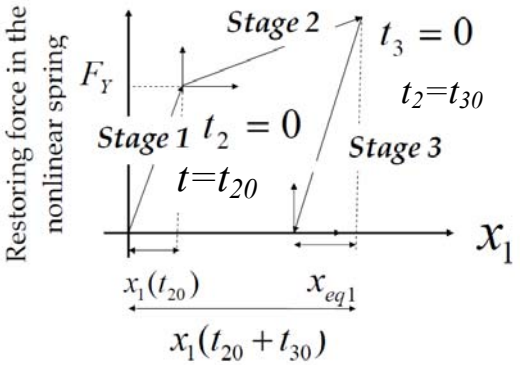

Figure 4: Three stages of the hysteretic half cycle

At Stage 1, the equation of motion will be same as in Equation (1) with the right hand term being zero. As the system was excited with an initial velocity profile proportional to the j^{th} mode, the initial conditions can be written as follows:

$$\{x_0\} = \{0\} \tag{2}$$

$$\{\dot{x}_0\} = v_0\{\phi_j\} \tag{3}$$

where v_0 is a constant proportional to the magnitude of initial velocity profile. Thus, the displacement vector is

$$\{x(t)\} = \sum_{r=1}^{n} \{\phi_r\}\eta_r \tag{4}$$

i.e.,

$$\{x(t)\} = \frac{v_0}{\omega_j}\sin(\omega_j t)\{\phi_j\} \tag{5}$$

In Equations (3)-(5), ϕ_j, η_j and ω_j respectively denote the mode shape, displacement and frequency corresponding to the j^{th} mode evaluated using the stiffness matrix at Stage 1 (i.e., initial stiffness matrix). The time at which the nonlinear spring exceeds the yield displacement is denoted by $t = t_{20}$ as shown in Figure 4. The displacement vector at t_{20} is given by

$$\{x(t_{20})\} = \frac{v_0}{\omega_j}\sin(\omega_j t_{20})\{\phi_j\} \tag{6}$$

Stage 2 begins at $t = t_{20}$. A new coordinate system is introduced here as $x^{(2)}$ and t_2 with $t_2 = t - t_{20}$ and $x^{(2)} = x - x(t_{20})$. The equation of motion for this stage can be expressed as follows:

$$[M]\{\ddot{x}^{(2)}\}+[K]\{x^{(2)}\}+[\hat{K}]\{x(t_{20})\}=-[M]\{\ddot{x}_g\} \tag{7}$$

where $[\hat{K}]$ is the stiffness matrix in Stage 2. The initial conditions corresponding to $t_2 = 0$ can be written as

$$\{x^{(2)}(t_2=0)\}=\{0\} \tag{8}$$

$$\{\dot{x}^{(2)}(t_2=0)\}=\{\dot{x}(t_{20}\}=\frac{v_0}{\omega_j}\cos(\omega_j t_{20})\{\phi_j\} \tag{9}$$

The expression for the displacement in the r^{th} mode (of Stage 2) can be obtained after the modal transformation of Equation (7). That is

$$\eta_r^{(2)}(t_2)=\frac{v_0}{\hat{\omega}_r}\cos(\omega_j t_{20})\sin(\hat{\omega}_r t_2)\{\hat{\phi}_r\}^T[M]\{\phi_j\}-\frac{\omega_j}{\hat{\omega}_r{}^2}v_0\sin(\omega_j t_{20})\{1-\cos(\hat{\omega}_r t_2)\}\{\hat{\phi}_r\}^T[M]\{\phi_j\} \tag{10}$$

Thus, the displacement in Stage 2 can be expressed as follows:

$$\{x^{(2)}(t_2)\}=\sum_{r=1}^{n}\{\hat{\phi}_r\}\eta_r{}^{(2)}(t_2) \tag{11}$$

where $\hat{\phi}_r$, η_r, $\hat{\omega}_r$ are the mode shape, modal displacement and frequency corresponding to the r^{th} mode in Stage 2, respectively. As the velocity $\dot{x}_1^{(2)}$ becomes negative, the system again starts following the initial stiffness and Stage 3 starts. It is assumed that this stage begins at $t_2 = t_{30}$. The displacement with respect to the coordinate system in Stage 2 is provided as follows:

$$\{x^{(2)}(t_{30})\}=\sum_{r=1}^{n}\{\hat{\phi}_r\}\eta_r{}^{(2)}(t_{30}) \tag{12}$$

The new coordinate system comprising of $x^{(3)}$ and t_3 is introduced as shown in Figure 4, where $t_2 = t - t_{20} - t_{30}$. The displacement vector in this coordinate system $\{x^{(3)}\}$ provides the displacement such that starting from an unstressed condition and following the initial stiffness, the same stiffness force vector as at time t_{30} can be achieved. Therefore, equating any stiffness force in Stage 3 with the initial stiffness multiplied by displacement in Stage 3 coordinate system, one can write

$$[k]\{x(t_{20})\}+[\hat{k}]\{x^{(2)}(t_{30})\}+[k]\{x-x((t_{20}+t_{30})\}=[k]\{x^{(3)}\} \tag{13}$$

Defining a new term x_{eq}, the following expressions are obtained:

$$[k]\{x(t_{20})\}+[\hat{k}]\{x^{(2)}(t_{30})\}=[k]\{x_{eq}\} \tag{14}$$

$$\{x^{(3)}\}=\{x_{eq}\}+\{x-x(t_{20}+t_{30})\} \tag{15}$$

The equation of motion at Stage 3 can be expressed as:

$$[M]\{\ddot{x}^{(3)}\}+[K]\{x^{(3)}\}=0 \tag{16}$$

The initial conditions at $t_3 = 0$ are defined as follows:

$$\{x^{(3)}(t_3=0)\}=\{x_{eq}\} \tag{17}$$

$$\{\dot{x}^{(3)}(t_3=0)\}=\{\dot{x}^{(2)}(t_{30})\} \tag{18}$$

This in turn provides the modal displacement and the structural displacement at Stage 3 as given in Equations (19) and (20).

$$\eta_r^{(3)}(t_3)=\{\phi_r\}^T[M]\{x_{eq}\}\cos(\omega_r t_3)+\frac{\{\phi_r\}^T[M]\{\dot{x}^{(2)}(t_{30})\}}{\omega_r}\sin(\omega_r t_3) \tag{19}$$

$$\{x^{(3)}(t_3)\}=\sum_{r=1}^{n}\{\phi_r\}\eta_r{}^{(3)}(t_3) \tag{20}$$

From the aforementioned formulation, the modal displacements and velocities at the third stage of the hysteretic semi-loop (half-cycle) can be obtained. Note that the (instantaneous) modal properties of the third stage are same as that of the first stage. This provides the estimates of remaining modal energy along with the energy dissipated at each mode.

PARAMETRIC STUDY

For an initial excitation in terms of velocity proportional to a particular mode, the measure of energy transfer from that particular mode as well as the energy dissipation can be obtained. A parametric study has been conducted in this section to study the influence of several parameters on the transfer and dissipation of energy. For this purpose, a ten degrees-of-freedom spring-mass structure is considered. The mass distribution is assumed to be uniform (i.e., 5000 kg) for all floors. The stiffness distribution is shown in Table 1 (data set 2). The spring connected to the support is assumed to display a bilinear behaviour as earlier considered with the yield displacement of 0.05 mm. Here, the initial excitation of the first mode is considered.

Table 1: Two different distribution of the stiffness and difference in successive eigenvalues

Stiffeness data set 1	
Stiffness distribution	Difference in eigen values
1300000	
1300000	23.04
2600000	52.18
2600000	85.15
1950000	66.60
1300000	134.39
650000	125.80
650000	227.35
325000	387.18
325000	629.72

Stiffeness data set 2	
Stiffness distribution	Difference in eigen values
1300000	
1300000	45.69
1300000	87.32
1300000	121.19
1300000	144.29
1300000	154.57
1300000	151.12
1300000	134.24
1300000	105.43
1300000	955.27

Figure 5 provides the energy retained in the first three modes in Stage 3 of each hysteresis half-cycle for a 90% stiffness degradation of the nonlinear spring and for an initial velocity of 476 m/s. From this figure, the following observations can be made: (1) Most of the energy of the first mode is dissipated and transferred after the first hysteretic half-cycle. Further, a steady state condition reaches after a couple of hysteretic cycle. (2) The transfer of energy occurs mostly from the first mode to the second mode after the first hysteretic half-cycle. The third or higher modes receive negligible amount of hysteretic energy as can be seen from the energy in the third mode (Figure 5). (3) The energy dissipation in the first hysteretic semi-loop is much higher than the transfer of energy to other modes.

The following sections deal with the influence of a) initial velocity, b) degradation of the stiffness, and c) separation of the eigenvalues on this energy transfer and dissipation.

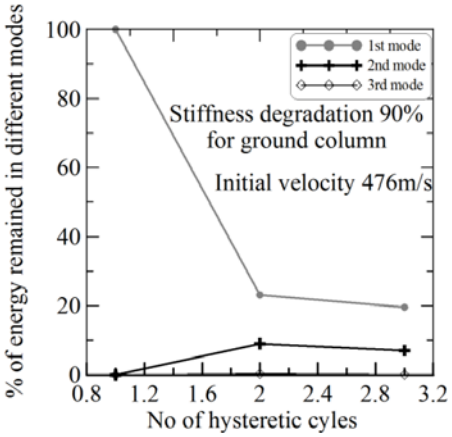

Figure 5: Energy in different modes along with the number of hysteretic half-cycles

Initial velocity

Figures 6(a) and 6(b) provide the plot of the energy remained in the first and second modes, respectively, with different hysteretic half-cycles. Here, the percentage energy is calculated with

respect to the total energy corresponding to the nominal velocity of 204 m/s. In addition to the observations made based on Figure 5, the following observations can be made from Figure 6.

1. At a lower velocity, the transfer of energy is much lower. As the velocity increases, the energy transfer also increases. The amount of energy dissipated is much higher than the energy transferred to the higher modes for all velocity ranges considered here in.
2. The energy retained in the first and second modes increases along with the increase in velocity.
3. A portion of the energy of the second mode (that was obtained from the first mode) gets dissipated in the next hysteretic half-cycle. After this the energy content of the second mode remains constant.

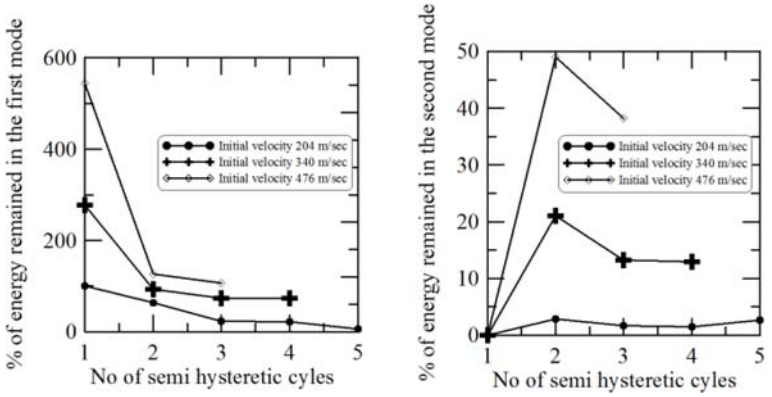

(a) (b)

Figure 6: Energy in the (a) first and (b) second mode for different velocity condition for a stiffness degradation of 90%

Stiffness degradation

Figures 7(a) and 7(b) describe the energy remained in different hysteretic half-cycles in the first and second modes, respectively for different amount of stiffness degradation for an initial velocity of 476m/s. One can note that for lower stiffness degradation, the percentage energy dissipated or transferred to the second mode is smaller. However, for higher stiffness degradation, the amount of energy dissipated or transferred to the second mode is significant.

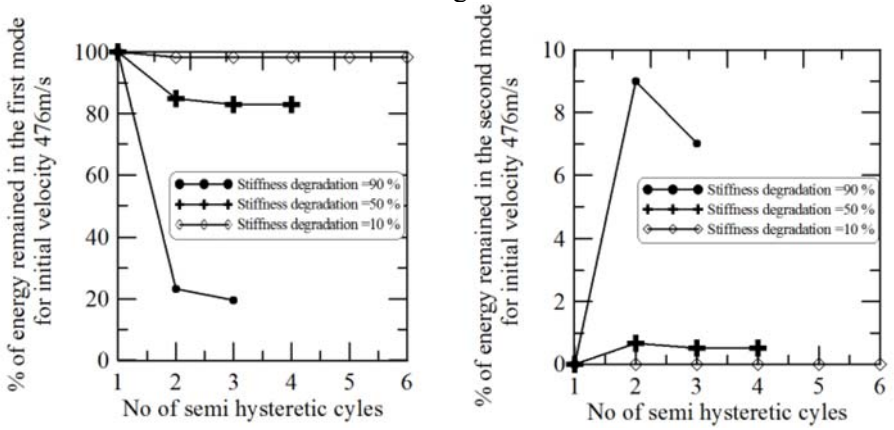

(a) (b)

Figure 7: Energy remained in the (a) first and (b) second modes for different amount of stiffness degradation

Closeness of eigenvalues

For a system with same overall stiffness and initial stiffness of the nonlinear spring, the stiffness distribution influences the spacing among the eigenvalues of the system. Here, two different stiffness distributions are considered. In the first case, the stiffness distribution is assumed to be uniform. For the first case, the spacing among the eigenvalues is higher for the lower modes and lesser for the higher modes. For the second case, the distribution considered is non uniform. In this, the stiffness for the first three springs are same as that of the first case. These stiffness are then distributed in a

gradually decreasing order. The stiffness and eigenvalue distributions are provided in Table 1 for two different dataset.

Figures 8(a) and 8(b) show the variation of energy remained for the first and second mode with number of hysteretic half-cycles considering an initial velocity of 476 m/s and stiffness degradation of 90%. It is observed from Figure 8(a) that for the fundamental mode, the closeness of eigenvalues does not influence the energy remained in this mode. However, the energy transferred to the second mode increases as the spacing of eigenvalues decreases (Figure 8(b)). In general, the closeness of eigenvalues, especially for the range considered here, does not influence the energy transfer phenomenon to a great extent.

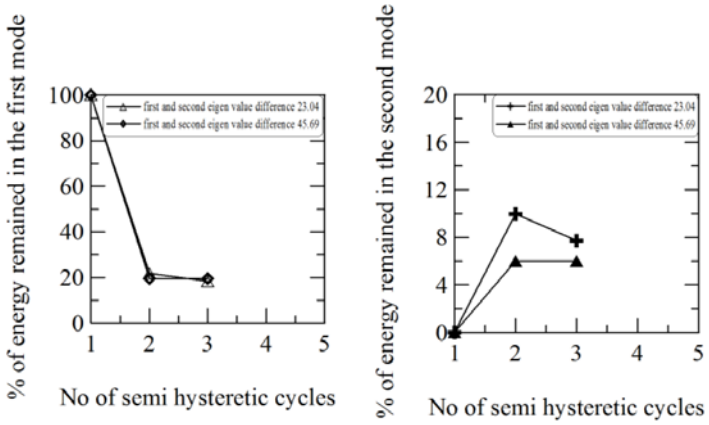

(a) (b)

Figure 8: Energy remained for different stiffness distributions: (a) first mode, (b) second mode

Sensitivity of different parameters

A sensitivity analysis is further carried out considering a) an increase in the initial velocity at a rate of 10% starting from 170m/s to 476 m/s and b) an increase in stiffness degradation starting from 10% to 90% of the initial stiffness of the nonlinear spring. Figure 9 shows the sensitivity of these two parameters. At lower stiffness degradation, the initial velocity is found to be a sensitive parameter influencing the energy remained in a particular mode (Figure 9(a)). However, at higher stiffness degradation, the initial velocity does not influence the energy remained in a mode. Almost all velocity ranges have same energy retained at a steady state condition as can be seen from Figure 9(a) for a stiffness degradation level of 90%. This is obvious for an elasto-plastic SDOF system, where the energy retained in steady state remains constant. On the other hand, for low stiffness degradation, the energy retained increases with the increase in initial velocity. This is because for low stiffness degradation, the system is closer to a linear system, where energy content increases with an increase in initial energy of excitation.

From Figure 9(b) one can notice that at a low velocity, the energy retained remains almost the same for all stiffness degradation. At a higher velocity, the retained energy decreases along with the increase in stiffness degradation. Therefore, the stiffness degradation significantly increases the energy retained in a particular mode.

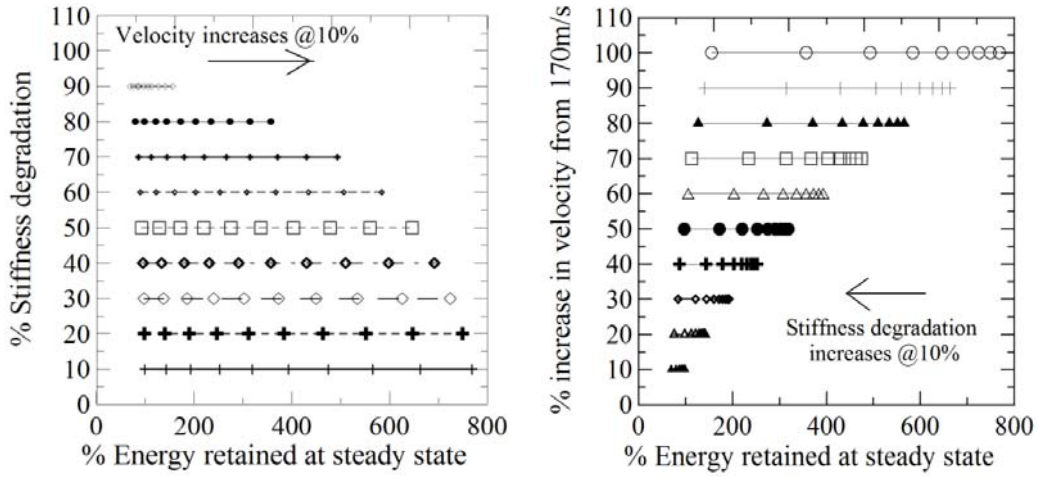

Figure 9: Variation of energy remained for (a) an uniform 10% variation of velocity at different stiffness degradations (b) an uniform 10% variation of stiffness degradation at different velocities

SIMPLIFIED EXPRESSION

In this section, simplified approximate expressions are derived for evaluation of energy dissipation and transfer to other modes. The eigenproperties of the degraded system are evaluated in terms of initial system properties (*Ray Chaudhuri*, *2008*). The i^{th} eigenvalue of the perturbed (degraded) system in terms of the initial eigenvalue and stiffness degradation can be expressed as follows:

$$\hat{\lambda}_i = \lambda_i \left[1 - (\phi_1^{(i)})^2 \frac{\delta k}{\lambda_i} \right] \tag{21}$$

where $\hat{\lambda}_i, \lambda_i$ are the perturbed and initial i^{th} eigenvalues of the system, respectively; Δk is the stiffness degradation of the spring closest to the support and $\phi_1^{(i)}$ is the 1st element of the i^{th} eigenvector (considering initial stiffness of the system). Similarly, the expression for the modal coupling term $\{\hat{\phi}_r\}^T [M] \{\phi_j\}$ can be written as follows:

for $r \neq j$

$$\{\hat{\phi}_r\}^T [M] \{\phi_j\} = \frac{\phi_1^r \phi_1^j \delta k}{\lambda_r - \lambda_j} \tag{22}$$

and for $r = j$

$$\{\hat{\phi}_r\}^T [M] \{\phi_j\} = 1 \tag{23}$$

Modal displacement and velocity at Stage 2

Considering the approximations for the perturbed eigen properties of the system, the modal displacement at the end of the Stage 2, i.e., $t_2 = t_{30}$ is provided as follows:

for $r \neq j$

$$\eta_r^{(2)}(t_{30}) = \frac{v_0}{\hat{\omega}_r} \left(- \frac{\phi_1^r \phi_1^j \delta k}{\lambda_r - \lambda_j} \right) \left[\cos(\omega_j t_{20}) \sin(\hat{\omega}_r t_{30}) - \frac{\omega_j}{\hat{\omega}_r} \sin(\omega_j t_{20}) \{ (1 - \cos(\hat{\omega}_r t_{20}) \} \right] \tag{24}$$

and for $r = j$

$$\eta_r^{(2)}(t_{30}) = \frac{v_0}{\hat{\omega}_j}\left[\cos(\omega_j t_{20})\sin(\hat{\omega}_r t_{30}) - \frac{\omega_j}{\hat{\omega}_r}\sin(\omega_j t_{20})\{(1-\cos(\hat{\omega}_r t_{20})\}\right] \tag{25}$$

Similarly, the modal velocity is provided by
for $r \neq j$

$$\dot{\eta}_r^{(2)}(t_{30}) = \left(\frac{\phi_1^r \phi_1^j \delta k}{\lambda_r - \lambda_j}\right) v_0\left[\frac{\omega_j}{\hat{\omega}_r}\sin(\omega_j t_{20})\sin(\hat{\omega}_r t_{30}) - \cos(\omega_j t_{20})\cos(\hat{\omega}_r t_{30})\right] \tag{26}$$

for $r = j$

$$\dot{\eta}_r^{(2)}(t_{30}) = v_0\left[\cos(\omega_j t_{20})\cos(\hat{\omega}_r t_{30}) - \frac{\omega_j}{\hat{\omega}_r}\sin(\omega_j t_{20})\sin(\hat{\omega}_r t_{30})\right] \tag{27}$$

Modal displacement and velocity at Stage 3

The modal displacement at Stage 3, i.e., at $t_3 = 0$ can be obtained as follows:

$$\eta_r^{(3)}(t_3 = 0) = \{\phi_r\}^T[M]\{x_{eq}\} = \{\phi_r\}^T[M]\{x(t_{20})\} + \{\phi_r\}^T[M][k^{-1}][\hat{k}]\{x^{(2)}(t_{30})\} \tag{28}$$

For $r \neq j$

$$\eta_r^{(3)}(t_3 = 0) = \{\phi_r\}^T[M]\sum_{m=1}^{n}\hat{\phi}_m\hat{\eta}_m(t_{30}) - \{\phi_r\}^T[M][k^{-1}][\Delta k]\sum_{m=1}^{n}\hat{\phi}_m\hat{\eta}_m(t_{30}) \tag{29}$$

where $[\Delta k] = [k] - [\hat{k}]$

Putting the approximation for $\{\hat{\phi}_r\}^T[M]\{\phi_j\}$ in the above expressions and neglecting some of the summation terms having a very negligible contribution towards the modal displacement, the following approximate expression is obtained for the modal displacement at Stage-3:

$$\eta_r^{(3)}(t_3=0) = \frac{\phi_1^r \phi_1^j \delta k}{\lambda_r - \lambda_j} v_0\left[\cos(\omega_j t_{20})\left(\frac{\sin(\hat{\omega}_j t_{30})}{\hat{\omega}_j} - \frac{\sin(\hat{\omega}_r t_{30})}{\hat{\omega}_r}\right) + \omega_j \sin(\omega_j t_{20})\left(\frac{\cos(\hat{\omega}_j t_{30})}{\hat{\omega}_j^2} - \frac{\cos(\hat{\omega}_r t_{30})}{\hat{\omega}_r^2}\right)\right]$$
$$+\frac{\phi_1^r \phi_1^j \delta k}{\lambda_r - \lambda_j} v_0 \omega_j \sin(\omega_j t_{20})\left(\frac{1}{\hat{\omega}_j^2} - \frac{1)}{\hat{\omega}_r^2}\right) - \frac{\delta k \phi_1^r \hat{\phi}_1^j}{\omega_r^2}\frac{v_0}{\hat{\omega}_j}\left\{\cos(\omega_j t_{20})\sin(\hat{\omega}_j t_{30}) + \frac{\omega_j}{\hat{\omega}_j}\sin(\omega_j t_{20})\cos(\hat{\omega}_j t_{30}) - \frac{\omega_j}{\hat{\omega}_j}\sin(\omega_j t_{20})\right\} \tag{30}$$

For $r = j$, a similar expression is

$$\eta_r^{(3)}(t_3 = 0) = \{\phi_r\}^T[M]\{x(t_{20})\} + \{\phi_r\}^T[M]\sum_{m=1}^{n}\hat{\phi}_m\hat{\eta}_m(t_{30}) - \{\phi_r\}^T[M][k^{-1}][\Delta k]\sum_{m=1}^{n}\hat{\phi}_m\hat{\eta}_m(t_{30}) \tag{31}$$

The approximate expression in terms of the initial states of the system can be expressed as:

$$\eta_r^{(3)}(t_3=0) = \frac{v_0}{\omega_j}\sin(\omega_j t_{20}) + \frac{v_0}{\omega_j}\left[\cos(\omega_j t_{20})\sin(\hat{\omega}_j t_{30}) - \frac{\omega_j}{\hat{\omega}_j}\sin(\omega_j t_{20})\{1-\cos(\omega_j t_{20})\}\right]$$
$$-\frac{\delta k \phi_1^j \hat{\phi}_1^j}{\omega_j^2}\frac{v_0}{\hat{\omega}_j}\left\{\cos(\omega_j t_{20})\sin(\hat{\omega}_j t_{30}) + \frac{\omega_j}{\hat{\omega}_j}\sin(\omega_j t_{20})\cos(\hat{\omega}_j t_{30}) - \frac{\omega_j}{\hat{\omega}_j}\sin(\omega_j t_{20})\right\} \tag{32}$$

In a similar manner, the expressions for the modal velocity can be obtained as follows:

$$\dot{\eta}_r^{(3)}(t_3=0)=\{\phi_r\}^T[M]\{\dot{x}_2(t_{30})\}=\{\phi_r\}^T[M]\sum_{m=1}^{n}\hat{\phi}_m\dot{\hat{\eta}}_m(t_{30}) \tag{33}$$

Using the approximation in a similar manner as for the modal displacement, the following expression is obtained for the modal velocity.

For $r \neq j$

$$\dot{\eta}_r^{(3)}(t_3=0)=\frac{\phi_1^r\phi_1^j\delta k}{\lambda_r-\lambda_j}v_0\left[\sin(\omega_j t_{20})\left(\frac{\sin(\hat{\omega}_r t_{30})}{\hat{\omega}_r}-\frac{\sin(\hat{\omega}_j t_{30})}{\hat{\omega}_j}\right)+\cos(\omega_j t_{20})\{\cos(\hat{\omega}_j t_{30})-os(\hat{\omega}_r t_{30})\}\right] \tag{34}$$

and for $r = j$

$$\dot{\eta}_r^{(3)}(t_3=0)=v_0\left[\cos(\omega_j t_{20})\cos(\hat{\omega}_j t_{30})-\frac{\omega_j}{\hat{\omega}_j}\sin(\omega_j t_{20})\sin(\hat{\omega}_j t_{30})\right] \tag{35}$$

The expressions for t_{20} can be written as

$$t_{20}=\frac{1}{\omega_j}\sin^{-1}\frac{a\omega_j}{v_0}\frac{1}{\phi_1^j} \tag{36}$$

Here, t_{30} has to be obtained from the following equation:

$$\hat{\phi}_1^j\left(\frac{\omega_j}{\hat{\omega}_j}\sin(\omega_j t_{20})\sin(\hat{\omega}_j t_{30})-\cos(\omega_j t_{20})\cos(\hat{\omega}_j t_{30})\right)=\sum_{r=2}^{n}\hat{\phi}_1^r\frac{\phi_1^j\phi_1^r\Delta k}{\lambda_r-\lambda_j}\left(\frac{\omega_j}{\hat{\omega}_r}\sin(\omega_j t_{20})\sin(\hat{\omega}_r t_{30})-\cos(\omega_j t_{20})\cos(\hat{\omega}_r t_{30})\right) \tag{37}$$

The term $\hat{\phi}_1^r$ and $\hat{\omega}_r$ can be approximated as

$$\hat{\phi}_1^r=\phi_1^r\left[1-\Delta k\sum_{\substack{p=1\\p\neq r}}^{n}\frac{(\phi_1^p)^2}{\lambda_r-\lambda_p}\right] \tag{38}$$

$$\hat{\omega}_r=\omega_r\sqrt{\left[1-(\phi_1^{(r)})^2\frac{\delta k}{\lambda_r}\right]} \tag{39}$$

From the expressions of modal displacement and velocity at the third stage, the modal energy can be obtained. As the energy in each mode except the one that was excited at the beginning is zero, the expressions derived above provides a direct estimate of the energy transferred to a particular mode from the first stage.

Result and Discussion

In order to evaluate the accuracy of simplified expression, the numerical example used for the parametric study is considered here with dataset 2 of Table 1. The results are obtained for a stiffness degradation of 30% and 70%. Figures 10 and 11 demonstrate the second stage modal displacement and velocity for the stiffness degradation of 30% and 70%, respectively. One can note that the predictions using the simplified expressions are quite good at this stage for the specified range of stiffness degradations. For higher stiffness degradation, minor deviations from the actual result can be observed.

Figures 12 and 13 display the prediction for modal displacement and velocity at the beginning of the third stage for stiffness degradation of 30% and 70%, respectively. It can be observed that for a lower degradation level, the prediction through simplified expressions gives very good estimate of response. However, for increased stiffness degradation, the prediction through simplified expressions deviates from the actual value for the modal displacements. This deviation decreases along with the increase in

the mode number as can be noticed for all the four plots (Figures 10-13). This is primarily because of the decreased modal interaction as a result of increased separation between the excited mode and any other mode. This can easily be understood from Equation (22). In general, one can conclude that the simplified expressions provide reasonable estimate of modal displacement and velocity at different stages of hysteresis for all the modes.

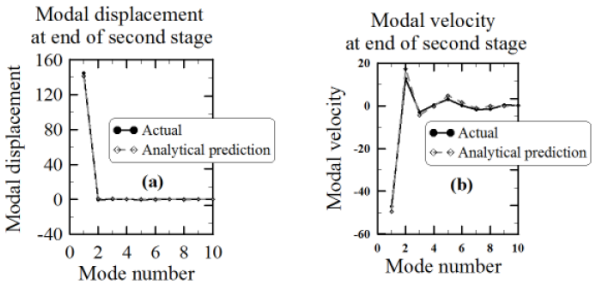

Stiffness degradation 30%

Figure 10: Comparison of the modal displacement and velocity at Stage-2 for a stiffness degradation of 30%

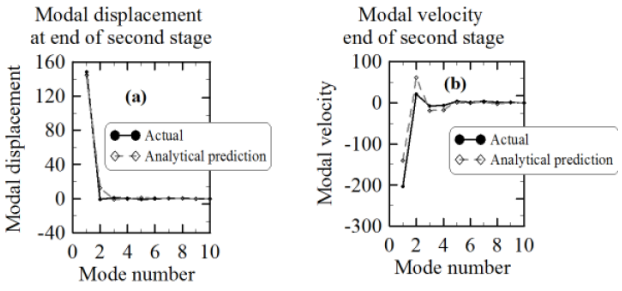

Stiffness degradation 70%

Figure 11: Comparison of the modal displacement and velocity at Stage-2 for a stiffness degradation of 70%

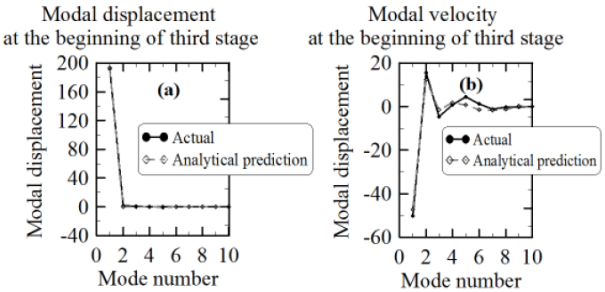

Stiffness degradatrion 30%

Figure 12: Comparison of the modal displacement and velocity at Stage-3 for a stiffness degradation of 30%

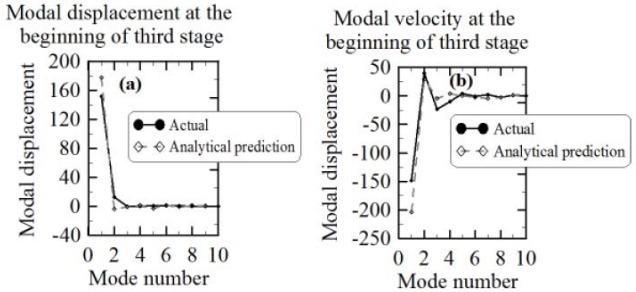

Stiffness degradatrion 70%

Figure 13: Comparison of the modal displacement and velocity at Stage-3 for a stiffness degradation of 70%

CONCLUSION

To understand the energy transfer phenomenon in a system undergoing hysteretic behaviour such as a base isolated building, in this study, a bilinear hysteretic behaviour is considered as a general case. A systematic study is carried out by formulating the equations of motions for different phases of motion. For this purpose, an un-damped multi-degree-of-freedom (MDOF) spring-mass system is considered. The stiffness of the spring connected to the base is assumed to possess a bilinear stiffness-degrading behaviour to represent the nonlinear behaviour as in the case of a base isolated structure. For simplicity, an initial velocity profile, proportional to the fundamental mode of the MDOF system, is considered and the free-vibration response of the system is studied. A numerical investigation is carried out on the influence of different parameters on the energy transfer to different modes of a building undergoing hysteresis. Further, simplified approximate expressions are also obtained using a perturbation approach for the modal displacement and velocity at different stages of hysteretic behaviour. The accuracy of the simplified expressions is then verified at different stages of the hysteretic cycle through a numerical study. Some of the findings of this study are as follows:

1. Most of the energy of the first mode is dissipated and transferred after the first hysteretic half-cycle. Further, a steady state condition reaches after a couple of hysteretic cycle.
2. The transfer of energy occurs mostly from the first mode to the second mode after the first hysteretic half-cycle. The third or higher modes receive negligible amount of energy.
3. The energy dissipation in the first hysteretic semi-loop is much higher than the transfer of energy to other modes.
4. At a lower initial velocity, the transfer of energy is much lower. As the velocity increases, the energy transfer also increases.
5. The energy retained in the first and second modes increases along with the increase in velocity.
6. For lower stiffness degradation, the percentage energy dissipated or transferred to the second mode is smaller. However, for higher stiffness degradation, the amount of energy dissipated or transferred to the second mode is significant.
7. The closeness of eigenvalues, especially for the range considered here, does not influence the energy transfer phenomenon to a great extent.

It is envisioned that the results of this study will provide a better understanding of the high-frequency responses that is observed for structures undergoing a sudden change in stiffness (such as a base isolated structure).

REFERENCES

Chakraborty S, Roy K, Chinta, C, and Ray Chaudhuri, S., (2012) “On development of a new seismic base isolation system”, *In the proceedings of the Sixth International Conference on Scalable Uncertainty Management (SUM 2012)*, Sept 17-19, Germany.

Ray-Chaudhuri, S., (2007) “Change in instantaneous eigen properties due to yielding of a structure”, *Journal of Sound and Vibration,* 312 (2008), 754–768

Ray-Chaudhuri, S, and Villaverde, R., (2008) "Effect of Building Nonlinearity on Seismic Response of Nonstructural Components: A Parametric Study", *ASCE Journal of Structural Engineering*, 134(4), 661-670.

Rodriguez, M. E., Restrepo, J. I., and Carr, A. J. (2002) “Earthquake-induced floor horizontal accelerations in buildings”, *Earthquake Engineering and Structural Dynamics*, 31(3), 693718.

Sewell, R. T., Cornell, C. A., Toro, G. R., McGuire, R. K., Kassawara, R. P., Singh, A., and Stepp, J.C. (1989) “Factors influencing equipment response in linear and nonlinear structures”, *Transactions of 9th International Conference on Structural Mechanics Reactor Technology*, 849-856.

Singh, M. P., Chand, T.-S., and Suarez, L. E. (1996) “Floor response spectrum amplification due to yielding of supporting structure”, *Proceedings of 11th World Conference on Earthquake Engineering*, Acapulco, Mexico.